Photometric cross-calibration of the SDSS Stripe 82 Standard Stars catalogue with Gaia EDR3, and comparison with Pan-STARRS1, DES, CFIS, and *GALEX* catalogues

Karun Thanjavur [ORCID],[1]★ Željko Ivezić [ORCID],[2] Sahar S. Allam [ORCID],[3] Douglas L. Tucker [ORCID],[3] J. Allyn Smith [ORCID][4]
and Stephen Gwyn[5]

[1]*Department of Physics and Astronomy, University of Victoria, 3800 Finnerty Road, Victoria, BC V8P 5C2, Canada*
[2]*Department of Astronomy and the DiRAC Institute, University of Washington, 3910 15th Avenue NE, Seattle, WA 98195, USA*
[3]*Fermi National Accelerator Laboratory, Batavia, IL 60510, USA*
[4]*Department of Physics, Engineering and Astronomy, Austin Peay State University, 601 College St., Clarksville, TN 37044, USA*
[5]*National Research Council, Canadian Astronomy Data Centre, Victoria, BC V9E 2E7, Canada*

ABSTRACT

We extend the SDSS Stripe 82 Standard Stars catalogue with post-2007 SDSS imaging data. This improved version lists averaged SDSS *ugriz* photometry for nearly a million stars brighter than $r \sim 22$ mag. With 2–3 times more measurements per star, random errors are 1.4–1.7 times smaller than in the original catalogue, and about three times smaller than for individual SDSS runs. Random errors in the new catalogue are $\lesssim 0.01$ mag for stars brighter than 20.0, 21.0, 21.0, 20.5, and 19.0 mag in *u*, *g*, *r*, *i*, and *z*-bands, respectively. We achieve this error threshold by using the Gaia Early Data Release 3 (EDR3) Gmag photometry to derive grey photometric zeropoint corrections, as functions of RA and Declination, for the SDSS catalogue, and use the *Gaia* BP–RP colour to derive corrections in the *ugiz* bands, relative to the *r*-band. The quality of the recalibrated photometry, tested against Pan-STARRS1, DES, CFIS, and *GALEX* surveys, indicates spatial variations of photometric zeropoints $\lessapprox 0.01$ mag (rms), with typical values of 3–7 millimag in the RA, and 1–2 millimag in the Declination directions, except for $\gtrsim 6$ millimag scatter in the *u*-band. We also report a few minor photometric problems with other surveys considered here, including a magnitude-dependent ~ 0.01 mag bias between $16 \leq G_{\mathrm{Gaia}} \leq 20$ in the Gaia EDR3. Our new, publicly available catalogue offers robust calibration of *ugriz* photometry below 1 per cent level, and will be helpful during the commissioning of the Vera C. Rubin Observatory Legacy Survey of Space and Time.

Key words: catalogues – instrumentation: photometers – methods: data analysis – standards – surveys – techniques: photometric.

1 INTRODUCTION

Modern multiband photometric sky surveys aim to deliver measurements uniform at or better than the 1 per cent (0.01 mag) level, to enable cosmological and other high-precision measurements (e.g. the Vera C. Rubin Observatory Legacy Survey of Space and Time; Ivezić et al. 2019). Photometric data are usually calibrated using sets of standard stars whose brightness is known from previous work. One of the largest catalogues with sub-percent measurement precision and optical multiband *ugriz* photometry was constructed by averaging multi-epoch data for about a million stars collected by the Sloan Digital Sky Survey (SDSS; York et al. 2000) in a 300 deg² region known as SDSS Stripe 82 (Ivezić et al. 2007, hereafter I007). The SDSS *ugriz* photometric system is now in use at many observatories worldwide and the I007 catalogue has been used both for calibration and testing of other surveys.

After completion of the I007 catalogue, SDSS obtained additional imaging data, about 2–3 times more measurements per star depending on its sky position within Stripe 82. This increased number of data points results in averaged photometry with 1.4–1.7 times smaller random errors (precision) than in the original catalogue (and about three times as small as for individual SDSS runs). In addition, the availability of photometric data from recent wide-field surveys such as the Dark Energy Survey (DES; Dark Energy Survey Collaboration et al. 2016), Pan-STARRS (PS1; Kaiser et al. 2010), and *Gaia* (Gaia Collaboration et al. 2018), enables a much more detailed and robust cross-calibration, including correcting for residual photometric zeropoint errors in SDSS flat-fielding. For example, Betoule et al. (2013) reported a saw-tooth pattern in photometric residuals between the SDSS and the Supernova Legacy Survey (SNLS) catalogues, as a function of Declination (see their fig. 23). Such a pattern is most likely due to errors in SDSS zeropoint calibration because of the flat-field correction of Stripe 82 being only a function of Declination (due to drift-scanning in RA direction). Given that systematic errors in other catalogues are much smaller (*Gaia*), or are expected to display different spatial patterns (DES and PS1), it is likely that a cross-comparison of several catalogues can result in significant improvements. These are the main reasons that motivated our decision to construct an updated version of the I007 catalogue.
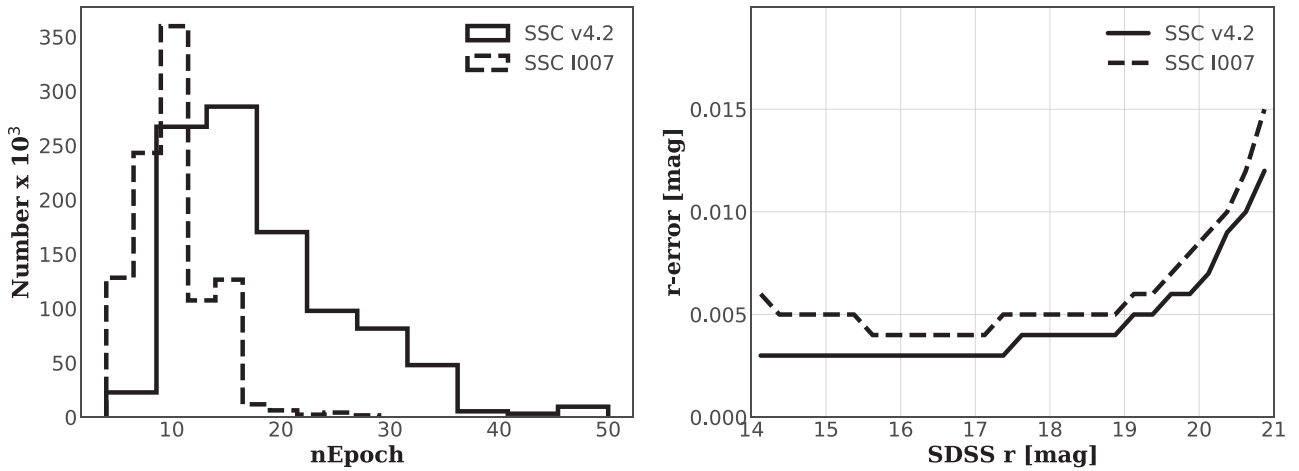

★ E-mail: karun@uvic.ca

Figure 1. (Left-hand panel) A comparison of the number of observational epochs for matched stars in the new standard star catalogue (SSC) v4.2 versus the I007 catalogue. (Right-hand panel) A comparison of the median formal *r*-band photometric uncertainties of matched objects in the v4.2 versus I007 catalogue, as a function of their mean *r* magnitudes.
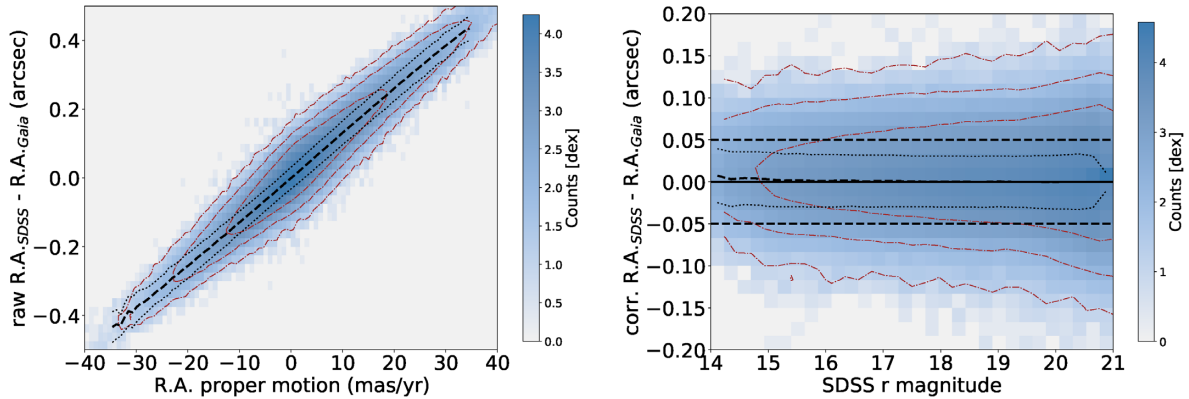

Figure 2. (Left-hand panel) The RA difference between SDSS and *Gaia* versus RA proper motion reported by Gaia EDR3. The solid line shows the median difference in bins of proper motion and the dashed lines mark the $\pm\sigma_G$ envelope around the medians, where σ_G is the robust standard deviation. The density of the distribution (in dex) is indicated by the colour bar, and the overplotted contours represent 1, 2, and 3 dex. (Right-hand panel) The RA difference after correcting using the best-fitting RA difference versus proper motion curve, as a function of the SDSS *r* magnitude. Overplotted contours represent 1, 2, and 3 dex. The residual differences are dominated by systematic errors in SDSS astrometry at the level of ∼28 milliarcsec (note that there is no increase with magnitude). In an analogous plot for Declination, the residuals are similar.

We describe data sets used in our analysis in Section 2, and the construction of the new catalogue and its analysis in Section 3. Our results are summarized and discussed in Section 4.

2 DATA SETS

2.1 SDSS Stripe 82 imaging data

In the SDSS survey, Stripe 82 is a contiguous, 300 deg^2 equatorial region, which stretches between $-60° \leq$ RA $\leq 60°$ [20–4h], and $-1°.266 \leq$ Dec $\leq 1°.266$. Following the initial, concerted effort by the SDSS collaboration between 2001 and 2008 to map this region repeatedly to a forecast imaging depth, $r \leq 22$, several other surveys in various wavebands have also targeted this same patch of sky to provide a rich multiwavelength data set suitable for a variety of investigations. SDSS observations have also continued in this region (e.g. the SDSS-II search for supernovae; Frieman et al. 2008), resulting in an imaging depth greater than what was initially planned.

Data from the SDSS imaging camera (Gunn et al. 1998) were collected in drift-scan mode. The images which correspond to the same sky location in each of the five photometric bandpasses (these five images are collected over ∼5 min, with an exposure time of 54 s for each band) are grouped together for simultaneous processing as a *field*. A field is defined as a 36 s (1361 rows) stretch of drift-scanning data from a single column of CCDs (sometimes called a *scan line*; for more details, see I007 and references therein).

2.1.1 The 2007 SDSS Standard Star catalogue

The SDSS standard star catalogue, I007 (version 2.6)[1] was constructed by averaging multiple SDSS photometric observations (at least four per band, with a median of 10) in the *ugriz* system. The catalogue includes 1.01 million non-variable stars. The

---

[1]This public catalogue is available by following the link provided in the data availability section.

measurements for individual sources have random photometric errors below 0.01 mag for stars brighter than 19.5, 20.5, 20.5, 20, and 18.5 in *ugriz*, respectively (about twice as good as for individual SDSS runs). Several independent tests of the internal consistency suggested that the spatial variation of photometric zero points is not larger than ~0.01 mag (rms).

2.1.2 Post-2007 SDSS data

In this work, we used the SDSS Data Release 15 (DR15) as available in 2019 April (Blanton et al. 2017). In DR15, the Stripe 82 region is covered by 118 *runs*, which include 32 292 fields, each with observations in the five *ugriz* SDSS filters. Using our programmatic query tool, we obtained the processed data for all these runs from the DR15 public data base.[2] In the data base, the data are presented as individual FITS tables, named `pho-toObj_<run>_<camcol>_<field>.fits`. From each fits table, we extracted photometric and astrometric quantities, time of observation, and several ancillary data for all the objects into a formatted master file for further processing.

The objects in each of these data files were then matched with the standard stars in the I007 catalogue using their mean sky positions (RA and Declination) and a matching radius of 0.5 arcsec. For matching, only deblended objects (*nchild*=0), lying between rows $64 < objc\_rowc \leq 1425$ in each field, were selected to avoid poor photometry due to blending or lying close to edges of the CCD. From these matched objects, only those with photometric error < 0.1 mag were selected to compute photometric zeropoint offsets between the I007 catalogue and DR15. These offsets were obtained independently for all runs and fields, in all five filters, and applied to bring our DR15 based catalogue to the same photometric scale as the I007 catalogue – in essence, we have re-calibrated photometry for all Stripe 82 runs in DR15 using the I007 catalogue. In addition, the MJD and fractional MJD of observation were computed using the median of the TAI values (the GPS based time reported by the SDSS Apache Point Observatory) for these matched objects. In the final step, the photometric, astrometric, and other details for each of these matched standard stars were written to independent (one per star) light curve files. Further processing of these light curves is described in Section 3.1.

The final data set, consisting of all the light curves in the five *ugriz* filters for the 1006 849 standard stars in the I007 catalogue resulted in ~20 GB of tabular data. To make file search and access fast, the data were chunked into sub-directories, each spanning 1° in RA, and 0°.1 in Dec. (a 'poor-man's' two-dimensional tree structure). These light curve data files can be made available as a single tarball by emailing the contact author.

2.2 Gaia Early Data Release 3 data

For our primary astrometric and photometric cross calibration, we use the Gaia Early Data Release 3 (EDR3) catalogue (Gaia Collaboration et al. 2021). *Gaia* is a European Space Agency (ESA) mission designed to map over a billion stars in the Milky Way and the Local Group in three dimensions, providing accurate proper motion and radial velocity measurements. Gaia Collaboration et al. (2016) provide a detailed overview of the *Gaia* mission (spacecraft, instruments, survey and measurement principles, and operations), while technical details for specific topics relevant to our work may
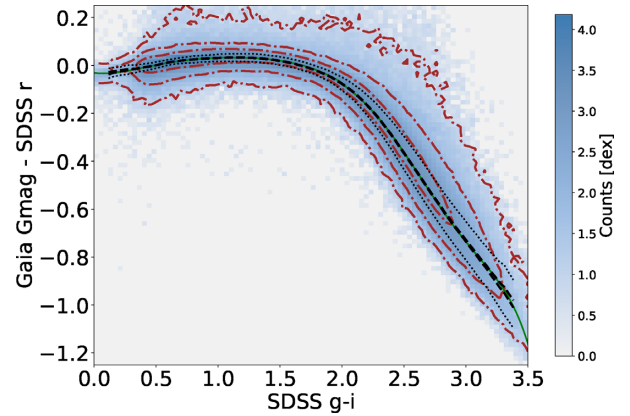
Figure 3. The variation of the difference between Gaia's G_{Gaia} magnitude from Early Data Release 3 and SDSS *r* magnitude with the SDSS $g − i$ colour. The colour map and contours illustrate the distribution of ~393 000 matched stars with $16 < G_{Gaia} < 19.5$. The thick dashed line represents the median values for 0.05 mag wide $g − i$ bins. These values are used to derive the grey zeropoint correction, as a function of RA and Declination. The thin dotted lines show the median values ± the robust standard deviation for each bin. The green solid line is a polynomial fit to the median values, given by equation (1) and discussed in Section 3.2.2. The fitted polynomial coefficients are listed in Table 1.

be found in the following citations: pre-processing and source-list creation (Fabricius et al. 2016), astrometric solution (Lindegren et al. 2018), processing the photometric data (Riello et al. 2018), photometric content and validation (Evans et al. 2018), and full catalogue validation (Arenou et al. 2018). A detailed description of *Gaia* data products may be found in Gaia Collaboration et al. (2018). Here, we summarize only the pertinent details.

EDR3 includes astrometry, photometry, radial velocities, and information on astrophysical parameters and variability, for approximately 1.8 billion sources.[3] This data set is based on the first 34 month of the mission and includes celestial positions and the apparent brightness in the broad-band G (G_{Gaia} hereafter) for sources brighter than $G_{Gaia} \sim 21$. This data release also contains two additional broad-band magnitudes, the BP (330–680 nm) and RP (630–1050 nm). Gaia EDR3 photometry is generally superior to ground-based photometry for sources with sufficient signal-to-noise ratio, and we use it to derive zeropoint corrections for SDSS photometry, as described in Section 3.2.

2.3 Dark Energy Survey (DES) data

The Dark Energy Survey (DES; Dark Energy Survey Collaboration et al. 2016) is an imaging survey of the Southern Galactic Cap in 5 filter passbands ($grizY_{DES}$) that was conducted from 2013 to 2019 with the 570 mega-pixel Dark Energy Camera (DECam; Honscheid & DePoy 2008; Flaugher et al. 2015) on the Victor M. Blanco 4-m telescope at the Cerro Tololo Interamerican Observatory.

For this paper, we made use of the DES Data Release 1 (DES DR1; Abbott et al. 2018; Morganson et al. 2018) public data set, which is based on the first 3 yr of DES observations. The DES DR1 object catalogue consists of ~400 million objects to a depth of 24.33, 24.08, 23.44, 22.69, 21.44 mag in $grizY_{DES}$ bands (*S/N* = 10σ). The DES DR1's photometric calibration is uniform at the sub-percent level (rms) for each of the five filter passbands over

Table 1. The best-fitting coefficients for equation 1.

Colour range	a_0	a_1	a_2	a_3	a_4	a_5	a_6
$0.0 < g - i < 2.0$	-0.0307	-0.0885	0.6632	-1.0179	0.7262	-0.2547	0.0337
$2.0 < g - i < 3.4$	9.6488	-8.4115	-7.9834	13.757	-7.0973	1.5993	-0.1351
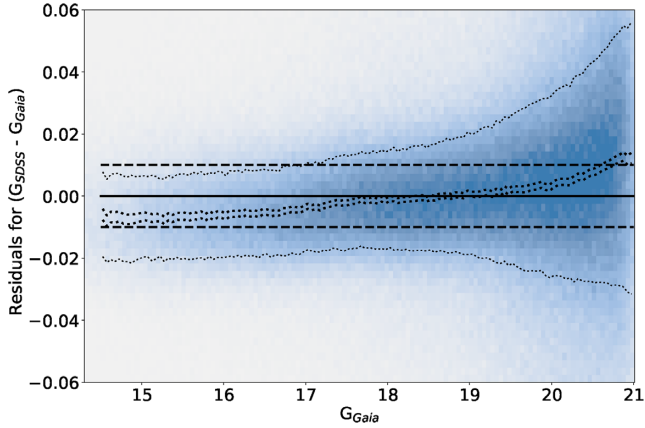
Figure 4. The variation of the residuals between *Gaia*'s G magnitude from Early Data Release 3, G_{Gaia}, and the synthetic G magnitude values, G_{SDSS} generated using SDSS *gri* photometry. The two solid lines represent the median values $\pm$ uncertainty of the median for each 0.05 mag wide G_{Gaia} bin. The short-dashed lines show the median values $\pm$ the robust standard deviation for each bin. The horizontal solid and long-dashed lines at zero and ± 0.01 mag, respectively, are added to guide the eye. Note an overall gradient of ~ 0.01 mag from bright ($G = 16$) to faint ($G = 20$) end – a comparison of the SDSS catalogue with Pan-STARRS and DES catalogues (see Fig. 16) suggests that its origin is a magnitude-dependent bias in Gaia's EDR3 photometry rather than a problem with SDSS photometry.
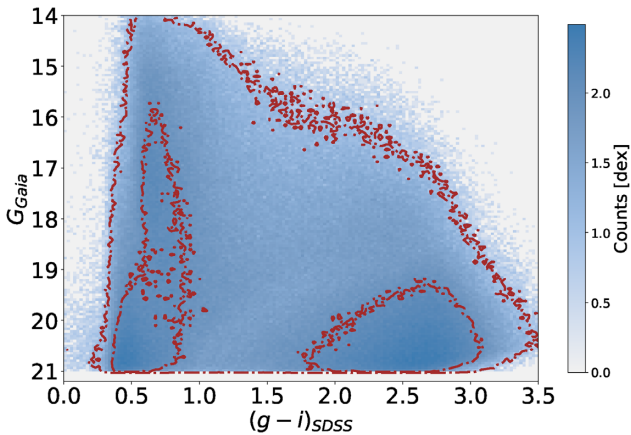
Figure 5. A Hess diagram constructed with Gaia's G magnitude and SDSS $g - i$ colour. The counts are shown on logarithmic scale, according to the colourbar. The 1σ and 2σ contours are also shown.

the entirety of the survey footprint. Its astrometric precision is quoted to be 151 milli-arcsec (rms). We downloaded DES DR1 data via the NOAO Data Lab[4] Table Access Protocol (TAP) service, selecting stars in the general area of the SDSS Stripe 82 region of the DES footprint. For the purposes of our analysis, we downloaded from the co-added catalogue, the weighted mean PSF magnitude

(WAVG_MAG_PSF) and magnitude error (WAVG_MAGERR_PSF) as well as the number of observations that went into the weighted catalogue-coadd weighted mean PSF magnitude (N_EPOCHS) in each filter band for each downloaded DES star. In total, 3585 229 stars were downloaded in the region (RA > 270° or < 105°; DEC $= -3°.5$ to $+3°.5$), of which 619 741 were matched to our SDSS catalogue using a match radius of 0.5 arcsec.

2.4 Pan-STARRS (PS1) data

The Panoramic Survey Telescope And Rapid Response System, Telescope 1 (Pan-STARRS-1, or PS1), commissioned in 2010, is the first of four planned 1.8-m telescopes, designed to map three quarters of the entire sky visible from Hawaii (Kaiser et al. 2010). This panchromatic, synoptic survey, called the 3π Steradian Survey was carried out in five bands, $grizy_{P1}$, with limiting magnitudes of 23.3, 23.2, 23.1, 22.3, and 21.4 mag. Chambers et al. (2016) provide full details about the PS1 observatory, the surveys being carried out, and an overview of the resulting data products. More detailed technical information on the following specific topics may be found in the following series of papers: the Pan-STARRS data processing system (Magnier et al. 2020a), pixel analysis, source detection and characterization (Magnier et al. 2020b), detrending, warping and stacking (Waters et al. 2020), photometric and astrometric calibration (Magnier et al. 2020c), and the data base and data products (Flewelling et al. 2020).

Here, we used the 2019 data release PS1-DR2 from *MAST*.[5] The catalogue overlapping the Stripe 82 region contains over 7 million point sources taken from the stacked 3π Steradian Survey. From the large set of measured and derived quantities available for these objects, we downloaded $grizy_{P1}$ PSF photometry and various quality flags. For this region, the mean positional uncertainties are 12 and 11 milli-arcsec in the RA and Dec directions. Based on this positional precision and that of our SDSS standard stars catalogue, we compared both catalogues using a matching radius of 0.5 arcsec. The resulting matched catalogue used in our analysis presented in Section 3.4 contains 909 000 objects. Taking the r band as being representative, the mean number of visits used to obtain the mean PSF magnitudes for these matched stars is 14 visits.

2.5 Canada-France Imaging Survey (CFIS) data

The Canada–France Imaging Survey (CFIS; Ibata et al. 2017) is a large observing programme being carried out at the Canada–France–Hawaii Telescope (CFHT) to map the northern sky in the MegaCam u and r bands. With a broad range of science goals, including providing ground-based optical photometry to complement the Euclid space mission, CFIS aims to cover 10 000 deg^2 in the u band to a depth of 24.4 mag. For our analysis, we were provided the u band data which overlaps the Stripe 82 footprint from the CFIS Data Release 2 (DR2; January 2020). In this region, CFIS data are available only
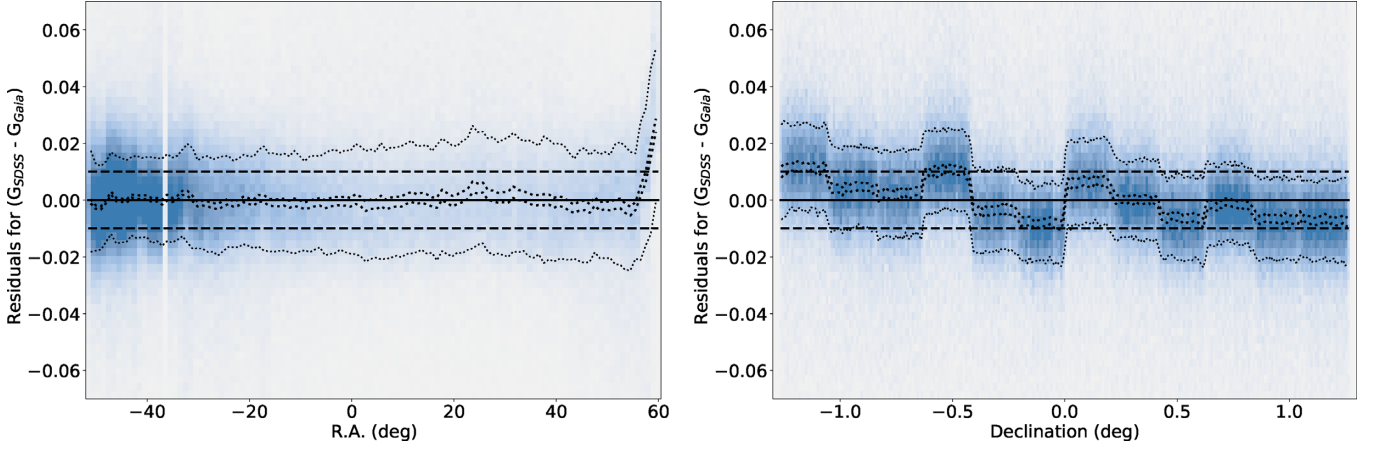
---

[4] http://datalab.noao.edu

[5] https://dx.doi.org/10.17909/T9RP4V

Figure 6. (Left-hand panel) The RA variation of the residuals between Gaia's G magnitude from EDR3, G_{Gaia}, and synthetic G magnitude values, G_{SDSS}, generated using SDSS *gri* photometry. The colour map illustrates the distribution of ~372 000 matched stars within $16 < G_{Gaia} < 19.5$ and $0.4 < g - i < 3.0$. The two solid lines represent the median values $\pm$ uncertainty of the median for $1°$ wide RA bins. The short-dashed lines show the median values $\pm$ the robust standard deviation for each bin. The horizontal solid and long-dashed lines at zero and ± 0.01 mag, respectively, are added to guide the eye. The mean of the two solid lines is the grey correction, as a function of RA, applied to the SDSS *ugriz* magnitudes. The standard deviation for the applied correction is 3.2 millimag. Note: The stripe of missing data seen at RA $\sim -37°$ is due to the presence of the globular cluster, *M*2. The resulting high stellar density region was masked off during data processing. (Right-hand panel) Analogous to the left-hand panel, except that here results are shown for $0°.01$ wide Declination bins. The 12 clearly visible regions correspond to two SDSS scans (in RA direction) and six CCD columns in the SDSS camera. The standard deviation for the applied correction is 6.5 millimag, with a maximum absolute value of ~0.01 mag.
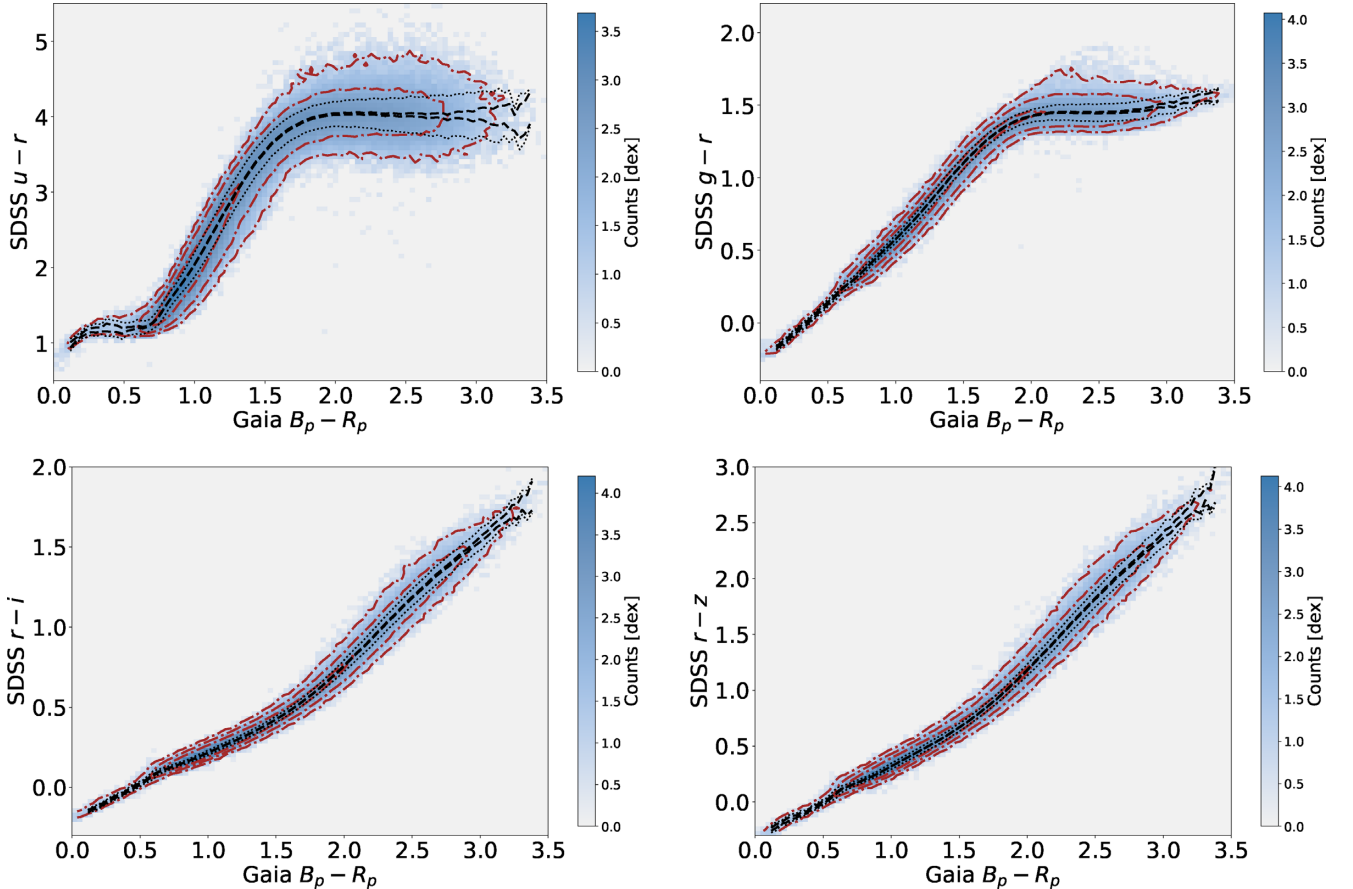
Figure 7. Analogous to Fig. 3, except that the correlations between SDSS colours and *Gaia*'s BP–RP colour are shown.
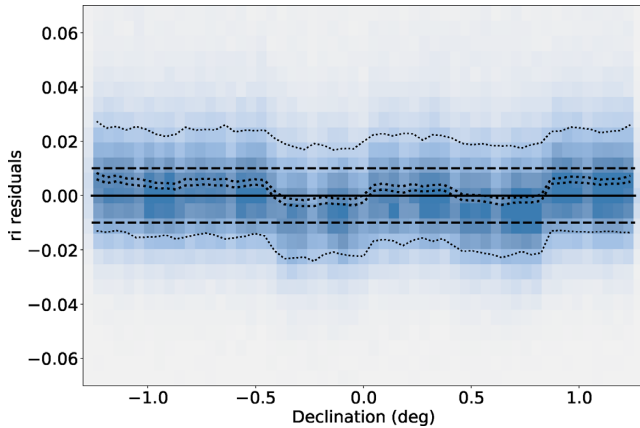
Figure 8. Analogous to Fig. 6 (right-hand), except that here residuals correspond to differences between the SDSS $r - i$ colour and a synthetic $r - i$ colour generated using *Gaia*'s BP−RP colour. Note the signature of SDSS camera columns at the level of a few millimags. The standard deviation for the binned medians is 3.2 millimag (for other bands, please see Table 2).

Table 2. The robust standard deviation for binned SDSS-based versus *Gaia*-based colour residuals[a].

Colour	rms for RA	rms for Dec.
Grey (Gmag)	3.2	6.5
$u - r$	0.0[b]	20
$g - r$	3.9	4.2
$r - i$	3.7	3.2
$r - z$	6.8	2.9

Notes. [a]The standard deviation for applied *Gaia*-based zeropoint corrections. The robust standard deviation is estimated using the interquartile range. The units are in millimag.
[b]For the *u* band, we could not confirm the RA behaviour of *Gaia*-based zeropoint correction with the CFIS data and did not apply it. The large *u* band correction as a function of Declination was validated with the CFIS data (see Section 3.5).

for Declination $> +0°\!\!.45$, thus covering only about a quarter of the Stripe 82 survey footprint.

The available CFIS DR2-Stripe 82 catalogue contains close to 965 000 sources, of which ∼315 000 matched within a link radius of 0.5 arcsec with stars in our SDSS standard stars catalogue. The astrometry over the complete CFIS survey region has been calibrated against Gaia DR2. The residuals of the astrometric solution are typically 10 mas. From the matched objects, we select only bright stars, $r \leq 20$ mag, with colours $1 \leq (u - g)_{SDSS} \leq 2.1$, following Ibata et al. (2017). This colour–magnitude cut yields 150 114 stars, which are used in the comparison described in Section 3.5.

2.6 *GALEX* data

The Galaxy Evolution Explorer (*GALEX*) all-sky survey catalogue in the *NUV* (1771–2831 Å) and FUV (1344–1786 Å) bands provides a unique photometric data set to crosscheck the *u* band of a multiband survey such as the SDSS. Processed and calibrated archival data from the 8 yr, All-sky Imaging (AIS) and Medium depth Imaging (MIS) surveys are available at *MAST*.[6] Due to the failure of the FUV detector midway through the survey, the available imaging depth in

[6]https://galex.stsci.edu/GR7/

this band is shallower by nearly 1 ABmag than the *NUV* depth of 20.8 ABmag in the AIS. Overall, the source number count in the FUV is, on average, only a tenth of that in the *NUV*. Given these limitations in the FUV survey, we extracted only sources in the *NUV* catalogue corresponding to the Stripe 82 footprint.

Bianchi, Shiao & Thilker (2017) provide full details of the *GALEX* survey, and we summarize only the *NUV* details, which are pertinent to our analysis here. The coverage over the survey region led to total exposure times of ∼150 s in the AIS and ∼1500 s in the MIS. The corresponding *NUV* survey depths are 20.8 and 22.7 ABmag in the two surveys, respectively. Objects in the Stripe 82 region were extracted and matched with our SDSS DR15 catalogue, described in Section 2.1.2 using a matching aperture radius of 3 arcsec, which corresponds to the matching radius used internally by *GALEX* to match their *NUV* and FUV sources. The *GALEX* catalogues do not list the RA, Dec. positional errors for their sources and we found their listed sky positions generally carry a greater uncertainty than the other catalogues used in this work.

Our matched *GALEX* catalogue consists of 150 945 *NUV* sources in the Stripe 82 footprint for which we obtained aperture magnitudes and uncertainties, as well as various fitted geometric measures for each of them. The astrometry has greater uncertainty than that of SDSS, with mean positional uncertainties of 1 arcsec rms. We also note that there is an overall mean shift in *GALEX* astrometry relative to that of the SDSS by −0.1 arcsec in RA and +0.3 arcsec in Dec.; our *GALEX*-SDSS positional offset results are comparable to what others have reported in the past (Agüeros et al. 2005; Morrissey et al. 2007; Heinis, Budavári & Szalay 2009; Bianchi, Conti & Shiao 2014). In addition, we find that the available depth in the Stripe 82 region is limited, with >80 per cent of the matched sample being brighter than $r = 18$ mag.

3 THE CONSTRUCTION AND ANALYSIS OF THE NEW V4.2 CATALOGUE

We first describe the construction of the new SDSS catalogue, v4.2, and the derivation of photometric zeropoint corrections using Gaia EDR3 data, and then compare the resulting photometry to Gaia EDR3, DES, Pan-STARRS, CFIS, and *GALEX* catalogues.

3.1 The construction of raw SDSS catalogue from light curves

Given the light-curve data files described in Section 2.1.2, we computed the median and mean magnitudes, their formal uncertainties and χ^2 (assuming constant brightness) for all stars, in all five bands. Due to more observational epochs in DR15, the new data are more sensitive to variability; following I007, we applied $\chi^2 < 3$ in the *gri* bands, as well as requirements for at least four epochs in the same three bands and the formal uncertainty of the mean *r*-band magnitude below 0.05 mag. These selection criteria recovered 98.5 per cent stars from the original catalogue, resulting in a new catalogue with 991 472 stars.

Fig. 1 compares the numbers of epochs for matched stars (left-hand panel) and their formal uncertainties of the mean *r*-band magnitude (right-hand panel). The new catalogue has about 2–3 times more measurements per star, depending on its sky position within Stripe 82. Consequently, formal photometric uncertainties ('random errors') are about 1.4–1.7 times smaller. Using *Gaia* photometry, we recalibrate the zeropoints in this catalogue, as explained in the following subsection. This new, recalibrated version of the SDSS standard star catalogue, v4.2, is publicly available by following the link provided in the data accessibility section. A detailed comparison
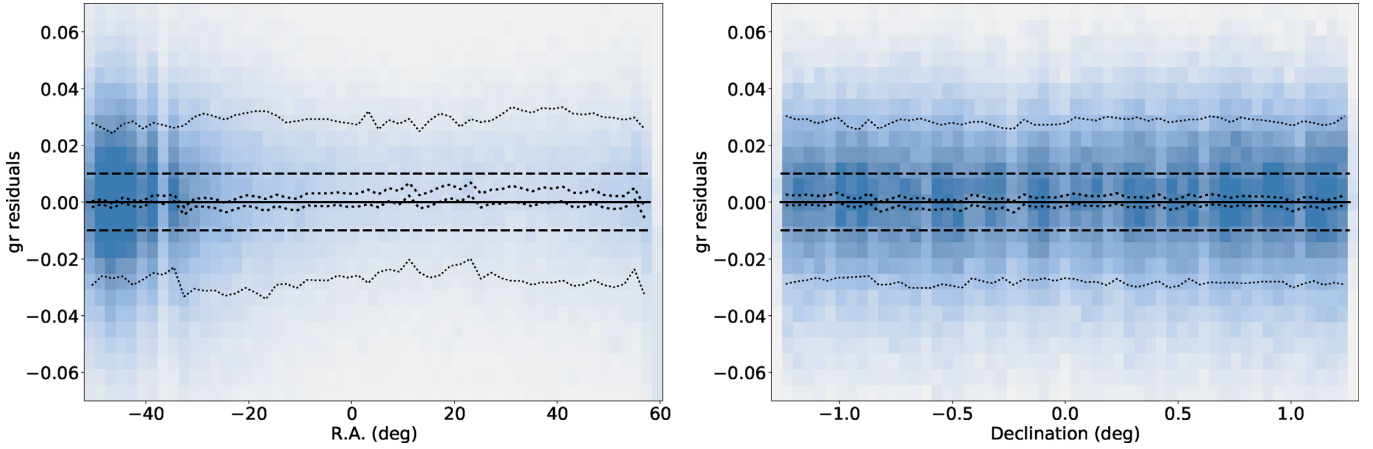
Figure 9. (Left-hand panel) Analogous to Fig. 6, except that here residuals between the SDSS $g - r$ colour from the v4.2 catalogue and a synthetic $g - r$ colour generated using *Gaia*'s BP−RP colour are shown. The binned median scatter is 1.6 millimag. (Right-hand panel) The SDSS $g - r$ residuals are shown as a function of Declination. The binned median scatter is 0.8 millimag.
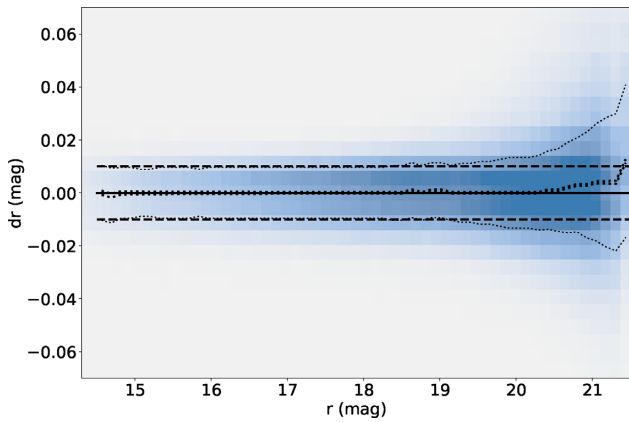

Figure 10. The differences between *r*-band magnitudes listed in the v2.6 and v4.2 SDSS Standard Star catalogues, shown as a function of the *r*-band magnitude. The scatter of median values per bin is 1.7 millimag. The scatter of individual values is ∼0.01 mag for $r < 20$ and is due to more data in the new catalogue.
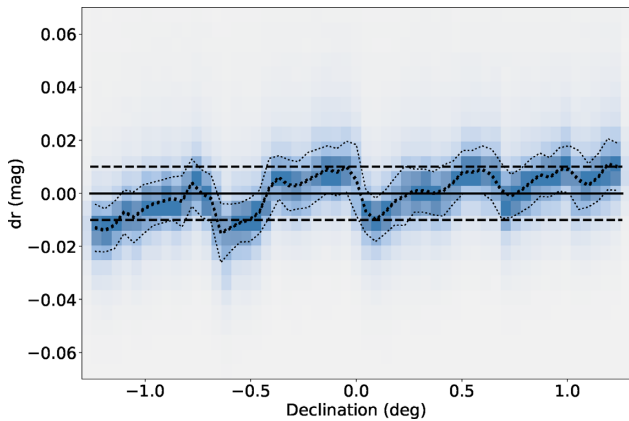
Figure 11. Analogous to Fig. 10, except that here the *r*-band differences are shown as a function of Declination (cross-scan direction). The size of the four regions corresponds to the size of the field of view of the SDSS Photometric Telescope (Tucker et al. 2006). The standard deviation for median values per bin is 7.1 millimag, with extreme values of about 0.01 mag. The scatter of binned medians in the RA direction is much smaller – 1.7 millimag. For statistics in other bands, please see Table 3.

Table 3. The robust standard deviation for magnitude differences between the v2.6 (old) and v4.2 (new) catalogues (in millimag).

Band	rms for RA	rms for Dec.
u	2.0[a]	25.5
g	4.0	9.7
r	1.7	7.1
i	4.1	6.5
z	7.5	8.4

Note. [a]For the *u* band, the scatter in the RA direction is due to more observations in v4.2 than in v2.6, rather than the zeropoint correction.

of the photometry between the old and new catalogues is discussed in Section 3.3.

3.2 The derivation of photometric zeropoint corrections using Gaia EDR3 data

The variation of photometric zeropoints with position on the sky in the I007 catalogue (see their equation 4) was constrained using a combination of stellar colours (the principal axes in colour–colour diagrams, for details see Ivezić et al. 2004) and a standard star network (Smith et al. 2002; Tucker et al. 2006). It is likely that residual errors in zeropoint calibration (e.g. a saw-tooth pattern as a function of Declination, which was reported by Betoule et al. 2013; see their fig. 23) could be further minimized using uniformly calibrated space-based photometry from Gaia EDR3, as shown in this work.

3.2.1 Positional matching of the SDSS and Gaia catalogues

Naively, one would positionally match the SDSS and Gaia EDR3 catalogues using a matching radius of about 0.3 arcsec because SDSS positions are accurate to better than 0.1 arcsec per coordinate (rms) for sources with $r < 20.5$ mag (Pier et al. 2003). However, observational epochs are sufficiently different that stellar proper motions need to be accounted for; indeed, we find a very strong correlation between the SDSS–*Gaia* positional differences and proper motions published in the Gaia EDR3 catalogue (see the left-hand panel in Fig. 2). After accounting for proper motions, the positions agree at the

level of ∼28 milliarcsec (robust[7] rms, per coordinate). The residual differences are dominated by systematic errors in SDSS astrometry because there is no increase of this rms with magnitude (see the right-hand panel in Fig. 2), and because the contribution of *Gaia*'s astrometric measurement uncertainties is negligible. The implied SDSS astrometric accuracy of ∼28 milliarcsec is substantially better than the 0.1 arcsec reported by Pier et al. (2003), but note that here we used positions 'averaged' over typically ∼20 SDSS runs (see the left-hand panel in Fig. 1).

3.2.2 Gaia-based photometric zeropoint corrections

Gaia EDR3 reported G_{Gaia} magnitudes, which approximately span the SDSS *griz* bandpasses, and BP and RP magnitudes, which approximately correspond to the blue and red halves of the G_{Gaia} bandpass. We first use G_{Gaia} data to derive 'grey' zeropoint corrections (applied to all five SDSS bands), and then use the BP–RP colour to derive zeropoint corrections for the *ugiz* bands, relative to the *r* band.

The basic idea is simple: first, use *Gaia*'s G magnitude, G_{Gaia}, and the SDSS *gri* magnitudes to derive a synthetic G magnitude, G_{SDSS} based on SDSS data, see Fig. 3. Next, bin the $\Delta G = (G_{SDSS} - G_{\mathrm{Gaia}})$ residuals by RA and Dec., and use the median residuals per bin as the grey correction for SDSS photometry (as functions of RA and Dec.). Similarly, use *Gaia*'s BP–RP colour to derive synthetic $u - r$, $g - r$, $r - i$, and $r - z$ colours, and use the median residuals per bin as zeropoint corrections for the *ugiz* bands.

Given a large number of matched stars (∼400 000), and a large number of colour combinations, we do not attempt to derive analytic fits for synthetic magnitudes and colours but instead use narrow colour bins of 0.05 mag, and linearly interpolate between the bins. We have verified that even sixth-order polynomial fits do not provide better results than this simple numerical approach. For example, we had to use two piece-wise polynomial fits to be able to fit the G_{Gaia}-r versus $g - i$ relation with residuals smaller than 0.01 mag separately for $0.0 < g - i < 2.0$ and $2.0 < g - i < 3.4$ ($g - i = 2.0$ approximately corresponds to M0 MK spectral type). These fit residuals are dominated by systematic errors, mainly the inability of even the sixth order polynomial to follow all the variations at the millimag level)

$$G_{\mathrm{Gaia}} - r = \sum_{k=0}^{k=6} a_k \, (g - i)^k. \qquad (1)$$

The best-fitting polynomial coefficients for both colour ranges are listed in Table 1 and the fit is shown by the green solid line in Fig. 3.

The variation of G magnitude residuals, ΔG, with G_{Gaia} (see Fig. 4) shows an overall gradient of ∼10 millimag from bright ($G = 16$) to faint ($G = 20$) end. A comparison of the SDSS catalogue with Pan-STARRS and DES catalogues (see Section 3.4 and Figs 14 and 16) strongly suggests that the origin of this discrepancy is a magnitude-dependent bias in Gaia's G_{Gaia} photometry, rather than a problem with the SDSS catalogue (offsets between the SDSS and DES photometry, are <2 millimag at $G_{\mathrm{Gaia}} \sim 20$, and <5 millimag when compared to Pan-STARRS).

Given these two features, we limit the calibration sample to the $16 < G_{\mathrm{Gaia}} < 19.5$ mag range. We further restrict calibration stars

---

[7]We use a robust estimator of the standard deviation computed as $\sigma_G = 0.741*(q_{75} - q_{25})$, where q_{25} and q_{75} are the 25 and 75 per cent quantiles; and the normalization factor 0.741 assures that σ_G is equal to the standard deviation for a normal (Gaussian) distribution.

to the $0.4 < (g - i)_{\mathrm{SDSS}} < 3.0$ colour range (approximately A0–M5 spectral range), yielding a sample of ∼372 000 stars (see Fig. 5 for the G_{Gaia} versus $g - i$ colour–magnitude diagram). The behaviour of the median G magnitude residuals per RA and Declination bin are shown in the left- and right-hand panels, respectively, of Fig. 6.

Except for a few degrees long region at the edge of Stripe 82 (RA > 55°), the SDSS photometric zeropoints are remarkably stable with respect to RA; the scatter is only 3.5 millimag. On the other hand, there are clear deviations in the Declination direction, which clearly map to the 12 scanning strips that fill Stripe 82. We note that discrepancies never exceed 0.01 mag (with a scatter of 6.2 millimag), which was the reported accuracy of the I007 catalogue. Thanks to a large number of stars in the sample, and well calibrated *Gaia*'s photometric zeropoints across the sky, we can now constrain SDSS zeropoints with a precision of about 1 millimag per 0°.01 wide Declination bin.

The residuals shown in the left- and right-hand panels of Figs 6 are applied as 'grey' zeropoint corrections to *ugriz* magnitudes, as functions of RA and Declination, to all 991 472 stars in the catalogue.

In the next re-calibration step, we derive synthetic $u - r$, $g - r$, $r - i$, and $r - z$ colours from *Gaia*'s BP–RP colour, using the same binning procedure as we used above for the $G_{\mathrm{Gaia}} - r$ versus $g - i$ variation (see Fig. 7). An example of colour residuals is shown in Fig. 8. The median residuals per RA and Declination bins are then used as zeropoint corrections for the *ugiz* bands. We required that the median offsets for all stars are vanishing and thus photometry in the new catalogue is on the same AB scale as the old catalogue (for related discussion, see Section 3.7). The robust standard deviation for all zeropoint corrections is listed in Table 2.

The largest corrections were derived for the *u* band. Given that *Gaia*'s BP–RP colour does not strongly constrain the *u*-band flux, we used the CFIS catalogue (see Section 2.5) as an independent cross check. We verified that zeropoint errors in the SDSS catalogue implied by *Gaia* and CFIS data agree at the level a few millimags in Declination direction, but found larger inconsistencies of ∼0.01–0.02 mag for RA bins. For this reason, we only applied the *u*-band correction in Declination direction. The plausible *u*-band zeropoint errors in the new catalogue are further discussed in Section 3.5.

3.2.3 Validation of recalibration

By construction, the new v4.2 catalogue should not show appreciable zeropoint residuals when binned by RA and Declination. We have verified this expectation for all colours used in the recalibration. For illustration, Fig. 9 shows such a test for the $g - r$ colour, with binned median scatter of the order 1 millimag.

3.3 Comparison of the SDSS I007 catalogue and the v4.2 catalogue

The v2.6 ('old') SDSS Standard Star I007 catalogue has been extensively used (e.g. Frieman et al. 2008), and here, we briefly analyse differences between the v4.2 ('new') and v2.6 magnitudes to inform future users about the consistency of the catalogues. In our analysis, we first compare the magnitudes of individual stars in the v2.6 and v4.2 catalogues, and bin the differences by RA, Declination, and magnitude.

On average, both catalogue versions are on the same magnitude scale (the median *ugriz* magnitude differences for all stars are zero by
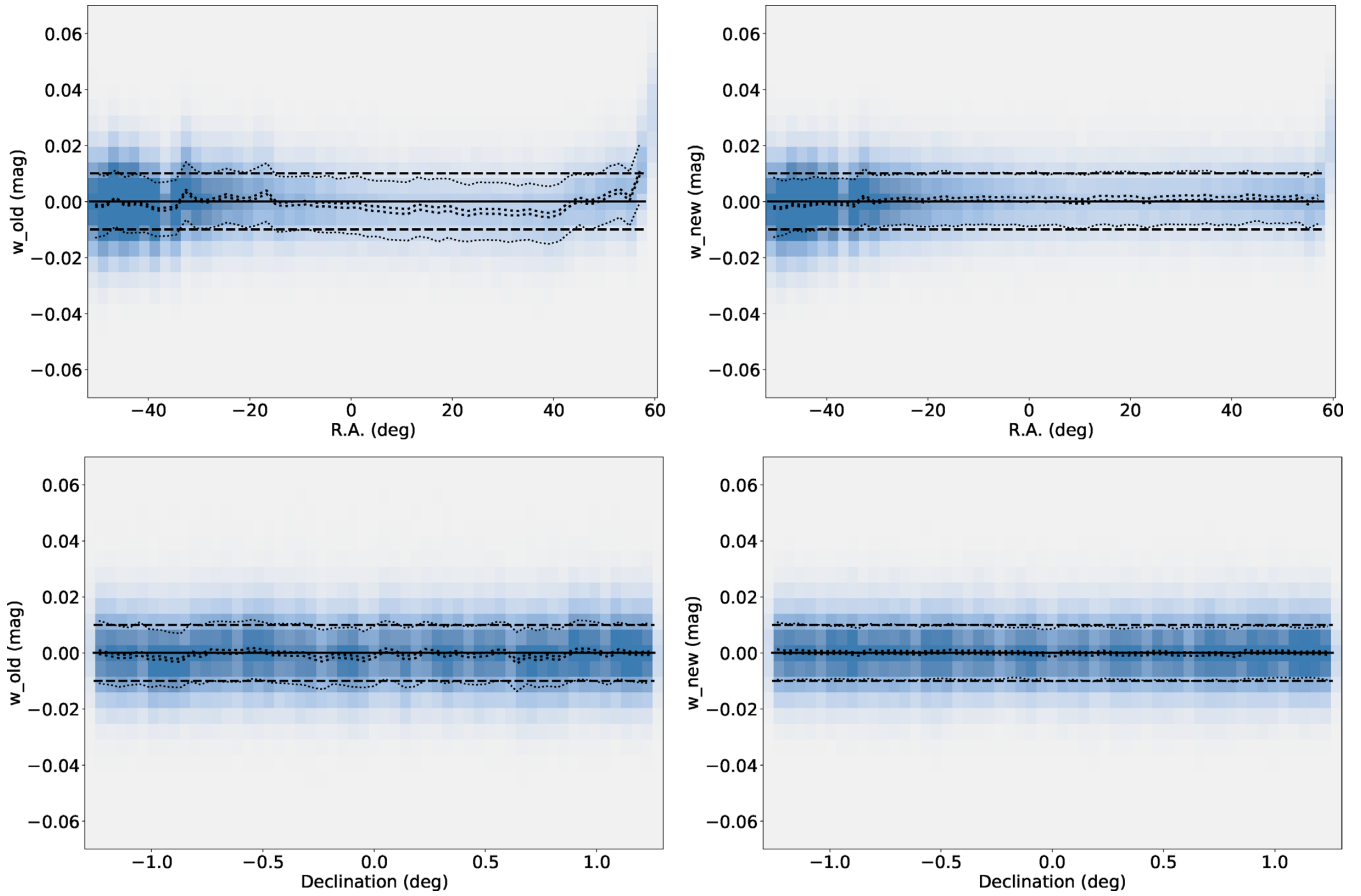
Figure 12. A comparison of the w colour, the second principal colour in the SDSS $r - i$ versus $g - r$ colour-colour diagram, for the v2.6 (*left-hand panels*) and v4.2 (*right-hand panels*) catalogues. The top row shows the behaviour in the RA direction, while the bottom row is for the Declination direction. The standard deviation of the median w values binned by RA and Dec. is 2.6 and 1.1 millimag for v2.6 and 1.0 and 0.3 millimag for v4.2, respectively.

construction). There are no systematic offsets when binned by magnitude, as illustrated in Fig. 10. The most obvious differences appear when magnitude differences are binned by Declination. An example is shown in Fig. 11, where the periodicity of residuals corresponds to the size of the field of view of the SDSS Photometric Telescope (Tucker et al. 2006). The standard deviation for median values per bin is 6.8 millimag, with extreme values of about 0.01 mag. It is likely that systematic errors in the photometry of the calibration star network were propagated through 'flat-field corrections' discussed by I007 to the v2.6 catalogue. We note that these errors, now found thanks to the *Gaia* catalogue, are well within the claimed photometric accuracy by both I007 and Smith et al. (2002). The standard deviation for the median values per bin for the five bands and both coordinates is listed in Table 3.

Given the quality of the *Gaia* photometry, there should be no doubt that SDSS *ugriz* photometry reported in the new v4.2 catalogue is superior to the old v2.6 catalogue. Nevertheless, we perform additional tests, based on the position of the stellar locus in the $g - r$ versus $u - g$, $r - i$ versus $g - r$ and $i - z$ versus $r - i$ colour–colour diagrams (Ivezić et al. 2004). The tests are based on the second principal colour for the blue part of the stellar locus, whose median should not deviate from zero by construction. Fig. 12 compares the behaviour of the w colour for the old v2.6 and new v4.2 catalogue and demonstrates that the *gri* photometry is better calibrated in the latter. The behaviour of the s and y colours for the new catalogue are shown in Fig. 13. The variation of s colour with RA is most likely affected by the variation of interstellar dust properties and stellar metallicity

distribution. *Based on these tests, we find that the contribution of the zeropoint errors is <5 millimag to gri photometry, and <10 millimag for the u and z bands.*

3.4 Comparison of the new v4.2 SDSS catalogue with DES and Pan-STARRS catalogues

The quality of photometric zeropoint calibration for the new SDSS catalogue can be conveniently tested with the DES (see Section 2.3) and Pan-STARRS (see Section 2.4) catalogues. Both catalogues list *griz* photometry of sufficient precision for essentially all stars from Stripe 82. Their photometric calibration procedures are expected to result in different spatial patterns and thus a cross-comparison with the v4.2 catalogue may reveal any residual problems with the zeropoint calibration. They are also deeper than the Gaia EDR3 catalogue and can thus provide further clues about the ~0.01 mag residual Gmag gradient (bright-to-faint end bias) illustrated in Fig. 4.

Our comparison of the magnitude differences binned in the RA and Declination directions are illustrated in Figs 14 and 15, respectively, and the corresponding robust standard deviations for binned median magnitude differences are listed in Table 4. This multi-survey comparison indicates that the spatial variation of photometric zero points in the updated SDSS catalogue is well below 0.01 mag (rms), with typical values of 3–7 millimag in the RA direction and 1–2 millimag in the Declination direction (excluding the z-band where these values are higher). Note the implied DES z-band zeropoint errors as a function of RA of up to 0.02 mag (see the bottom left-
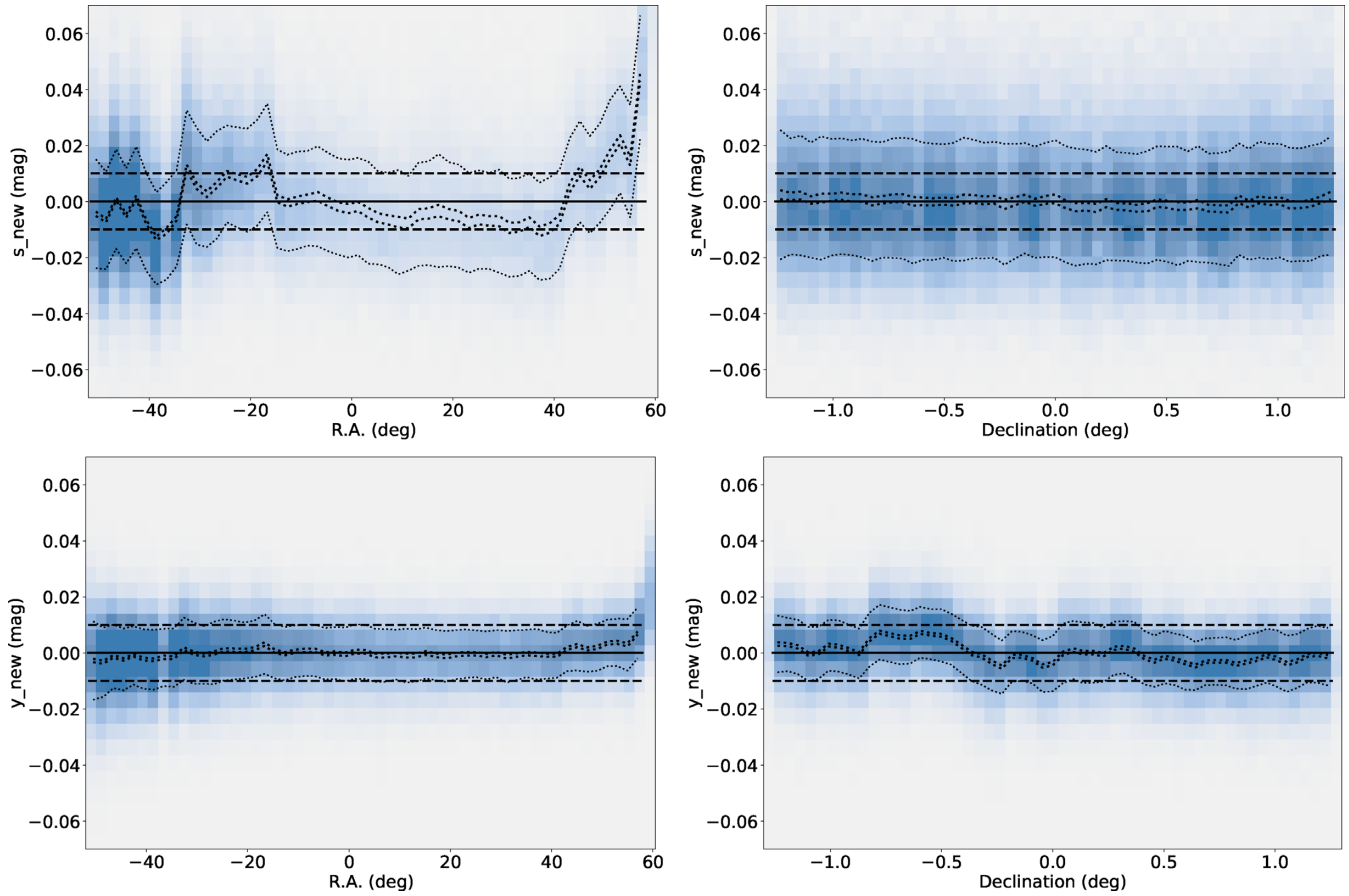
Figure 13. The behaviour of the *s* colour (top two panels), the second principal colour in the SDSS $g - r$ versus $u - g$ colour-colour diagram, and the *y* colour (bottom two panels), the second principal colour in the SDSS $i - z$ versus $r - i$ colour-colour diagram, for the new v4.2 catalogue. The standard deviation of the median *s* values binned by RA and Declination is 9.8 and 1.3 millimag, respectively, and 1.8 and 3.4 millimag for the *y* colour.

hand panel in Fig. 14), although a similar trend in the corresponding Pan-STARRS plot (bottom right-hand panel in Fig. 14) indicates that the SDSS catalogue, calibrated using Gaia EDR3, may be at least partially responsible for the observed differences[8]

The variation of the residual magnitude differences with magnitude (see Fig. 16 for DES results) is typically flat to within ∼3–4 millimag for both DES and Pan-STARRS. This much smaller gradient than the one observed for *Gaia* (∼20 millimag) implies a likely problem (a bias between bright and faint ends) with the Gaia EDR3 photometry. The largest discrepancy of about 2 millimag/mag is observed for the Pan-STARRS *r* band, while the gradient is limited to <1 millimag when compared to the DES *r* band.

3.5 Comparison of the new v4.2 SDSS catalogue and *u*-band data from the CFIS catalogue

The comparison of the new SDSS catalogue with the DES and Pan-STARRS catalogues in the previous section did not include the *u* band. To assess the quality of *u*-band zeropoint calibration, we use the CFIS catalogue (see Section 2.5). The CFIS *u*-band photometry was calibrated using a combination of the SDSS, Pan-STARRS, and *GALEX* UV data. Even given that we recalibrated the new SDSS catalogue using *Gaia* data, it should not matter for this comparison

that SDSS data were used in the calibration of the CFIS catalogue. Nevertheless, this should be kept in mind while interpreting the results presented in this section. We also note that the transmission curve of the MegaCam *u*-band filter used for the CFIS survey differs from that of the SDSS *u*-band filter.[9] However, this does not lead to any noticeable differences in the magnitude comparisons between the two catalogues presented here.

A comparison for about 150 000 sufficiently bright stars, $r < 20$, with colours matching the main sequence, $1.0 < u - g < 2.1$, is illustrated in Fig. 17. The binned median scatter for the Declination direction is 5.7 millimag with systematic differences of up to 0.01 mag. The constraints in the RA direction are noisier, with residuals appearing about twice as large as in the Declination direction. These residuals compare favourably to the results of the analysis by Ibata et al. (2017), who showed that some SDSS runs in Data Release 13 have *u*-band zeropoint errors as large as 0.1 mag.

3.6 Comparison of the new v4.2 SDSS catalogue and transformed *NUV* data from the *GALEX* catalogue

We also use the *NUV* magnitudes from *GALEX* (see Section 2.6) to provide an independent check on the SDSS *u*-band magnitudes, following the zeropoint corrections with *Gaia* photometry described

---

[8]For a comparison of DES DR1 and Gaia DR2 calibrations, see e.g. Fig. 9 of Abbott et al. (2018).

[9]https://www.cadc-ccda.hia-iha.nrc-cnrc.gc.ca/en/megapipe/docs/filt.html
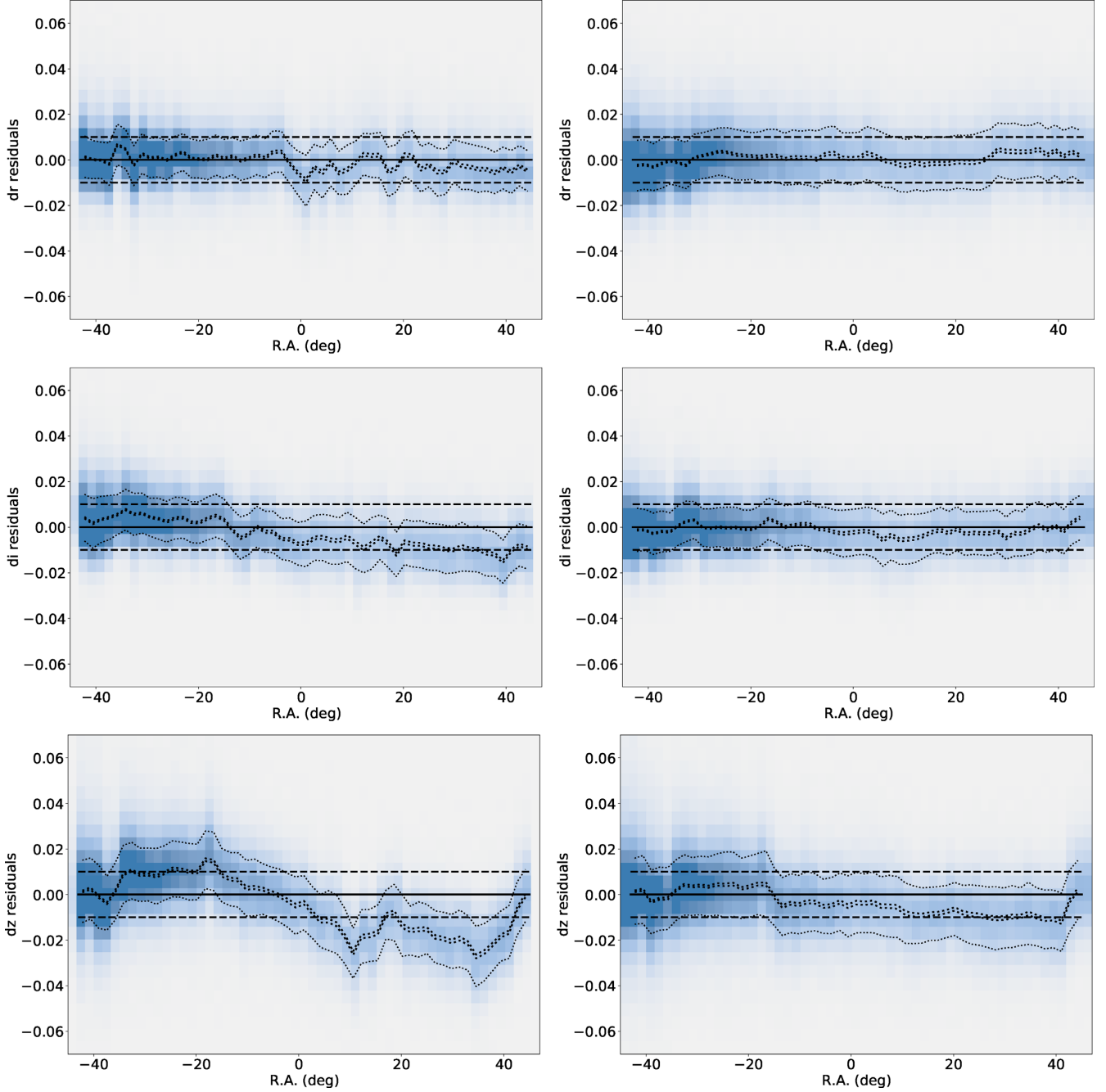
Figure 14. A comparison of the magnitude differences between the SDSS v4.2 catalogue and DES (left-hand panel) and Pan-STARRS (right-hand panel) catalogues, for the *riz* bands binned by RA.

in Section 3.2. For this, we derive the following *GALEX* to SDSS *u* transformation equation

$$
\begin{aligned}
u_{\text{est}} = \ & NUV - 0.990 \times (NUV - g) + 0.014 \times (NUV - g)^2 \\
& - 0.407 \times (g - i) + 0.797 \times (g - i)^2 + 0.835 \\
& + T \times [-1.346 \times (E(B - V) - 0.15 \\
& + 3.400 \times (E(B - V) - 0.15)^2],
\end{aligned} \tag{2}
$$

where *NUV* refers to *GALEX*, and *g* and *i* are SDSS magnitudes. *T* is a step function in the value of the interstellar reddening, $E(B–V)$,

from the Schlegel, Finkbeiner & Davis (1998) reddening map

$$
T = \begin{cases} 0 & E(B - V) \le 0.15 \\ 1 & 0.15 < E(B - V) < 0.3. \end{cases} \tag{3}
$$

This transformation relation, which is suitable for stars with $0.5 < (u - g)_{\text{sdss}} < 2.0$, $0.2 < (g - r)_{\text{sdss}} < 0.8$, $0.3 < (g - i)_{\text{sdss}} < 1.0$, and $E(B - V) < 0.3$, has a per star rms of $\sigma = 0.061$ mag (the relatively high rms is due in part to the relatively high rms in the *GALEX NUV* magnitudes). This relation converts the *GALEX NUV* magnitudes into very reasonable approximations of the SDSS *u*-band. To refine these approximations, we then applied the same sort of numerical transformation that was used for the SDSS to *Gaia* transformation
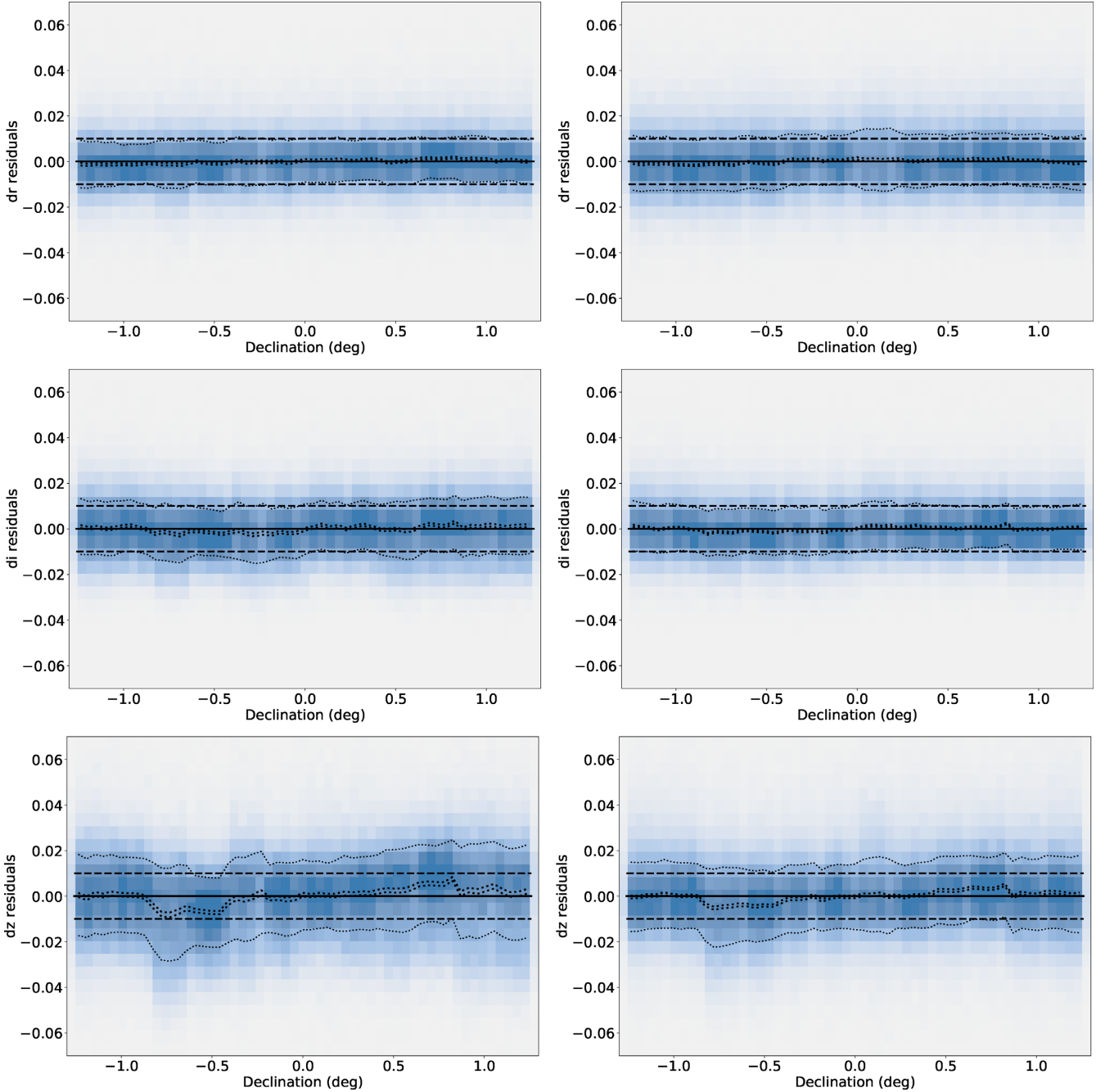
Figure 15. Analogous to Fig. 14, except that the magnitude differences are binned by Declination.

Table 4. The robust standard deviation for the binned median magnitude differences between the new v4.2 SDSS catalogue, and DES and Pan-STARRS1 catalogues (in millimag).

Band	DES RA	DES Dec.	PS1 RA	PS1 Dec.
g	4.8	2.0	3.3	1.6
r	3.3	0.9	2.1	0.9
i	5.9	1.4	2.2	1.0
z	12.1	3.6	5.1	2.3

in Fig. 3; this improved the overall per star rms to $\sigma = 0.055$, with most of the improvement occurring for the bluest, $(u - g)_{sdss} \lesssim 1.0$, and the reddest, $(u - g)_{sdss} \gtrsim 1.0$ stars in our sample.

Despite the relatively noisy results, we can make several conclusions based upon the binned data consisting of 89 722 matches between the v4.2 SDSS catalogue and the *GALEX* catalogue. First, in Fig. 18, we show the difference between the SDSS-measured and *GALEX*-predicted u_{sdss} versus SDSS u_{sdss} for the 80 053 matches that lie within the colour and $E(B-V)$ cuts used for the initial transformation equation (equation 1). Although the relation, even when binned like here, is noisy, there is clearly a noticeable trend in the residuals versus SDSS u. As with the comparison with *Gaia* (Fig 4), we expect that this magnitude dependence is associated with the *GALEX* photometry rather than with SDSS. Secondly, in Fig. 19
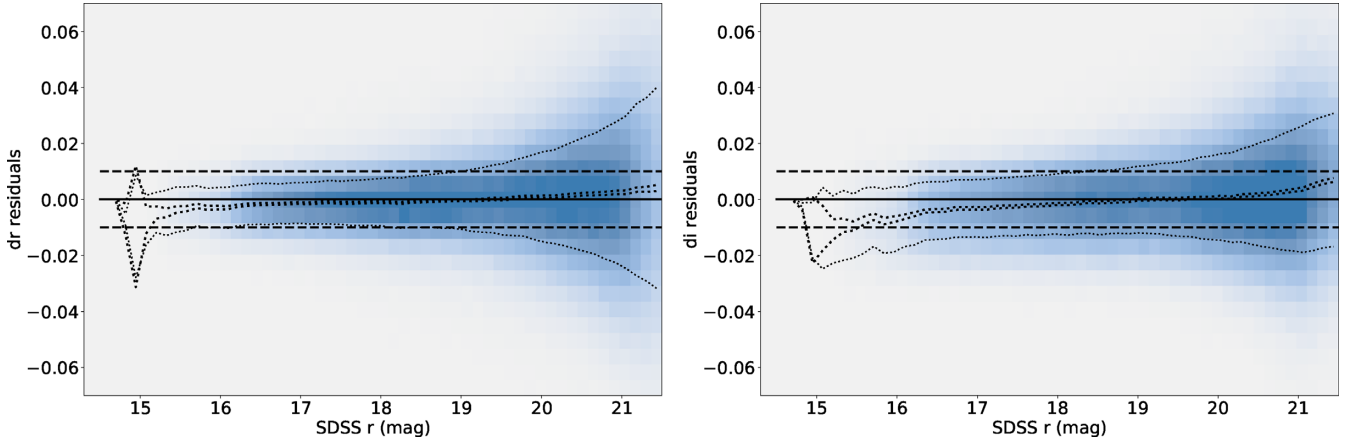
Figure 16. A comparison of the magnitude differences between the SDSS v4.2 catalogue and the DES catalogue, for the *r* and *i* bands. Note the very small gradient of the median residuals between the bright and faint ends: about 3–4 millimag and thus much smaller than ∼20 millimag when compared to the *Gaia G* magnitude (see Fig. 4).
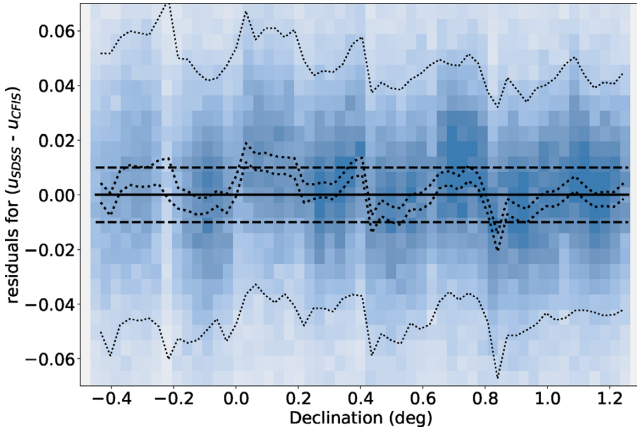
Figure 17. Analogous to Fig. 6 (right-hand panel), except that here residuals between the SDSS *u*-band magnitudes and *u*-band magnitudes from the CFIS catalogue (corrected for small colour terms, ∼0.05 mag, as a function of the $u - g$ colour), for ∼150 000 matched stars with $1.0 < u - g < 2.1$ and $r < 20$ are shown. The binned median scatter is 5.7 millimag. Note that the CFIS data are available only for Declination $> +0°.45$.
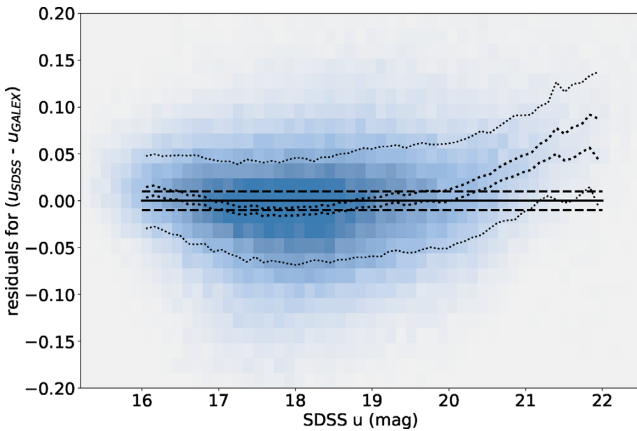
Figure 18. Analogous to Fig. 4, except that here the residuals between the SDSS *u*-band magnitudes and predicted *u*-band magnitudes transformed from the *GALEX* catalogue are shown. The individual star scatter is 54.5 millimag (dot–dashed lines); the binned median scatter is 24.5 millimag solid grey lines).

(left-hand panel), we plot this magnitude difference versus RA along SDSS Stripe 82. Here, in addition to the cuts used for Fig. 18, we also apply a cut of $u_{\rm sdss} \leq 20.0$, to avoid the worst deviations seen in that figure; this results in a sample of 69 783 matches. We do note some small but significant large-scale trends with RA, at the 9.5 millimag level (rms). Third and finally, in Fig. 19 (right-hand panel), we plot this magnitude difference versus DEC across SDSS Stripe82 using the same sample of 69 783 matches used for Fig. 19 (left-hand panel). Unlike for the CFIS comparison in the previous section (see e.g. Fig. 17), the *GALEX* comparison covers the full Dec. range of Stripe 82. Overall, aside of a possible slight gradient, there appear to be no strong large-scale trends. The hints of smaller scale, ∼0°.4 variations – roughly on the scale of a SDSS camera column – seen in the CFIS comparison (Fig. 17), however, are not seen here, perhaps due to the relative 'noisiness' of the *GALEX* comparison.

3.7 Offsets from AB magnitude scale

We estimate offsets from the AB magnitude scale using synthetic photometry derived from the spectra of three DA white dwarfs observed by *HST* (see Table 5): GD50 (specifically, the calibrated spectrum file gd50_004.fits) from the *HST* CalSpec data base of spectrophotometric standard stars (Bohlin, Gordon & Tremblay 2014),[10] and SDSSJ 232941.32+001107.8 and SDSSJ 010322.19–002047.7 from Narayan et al. (2019; the flux-calibrated modelled spectrum files were provided by G. Narayan, private communication). These three spectrophotometric calibrators are particularly useful for our purposes since they are faint enough not to be saturated in the SDSS photometry ($r > 14$) and they lie within the SDSS Stripe 82 footprint, making direct comparison to the SDSS measurements relatively simple. Synthetic AB magnitudes for these three DA white dwarfs were derived via numerical integration of equation (8) of Fukugita et al. (1996), which serves to define broad-band AB magnitudes. This equation requires not only a well-calibrated spectrum, but also the well-calibrated bandpass response curves for the photometric system in question. Here, we make use of the SDSS bandpass response curves from Table 4 of Doi et al.

[10]https://www.stsci.edu/hst/instrumentation/reference-data-for-calibration-and-tools/astronomical-catalogs/calspec
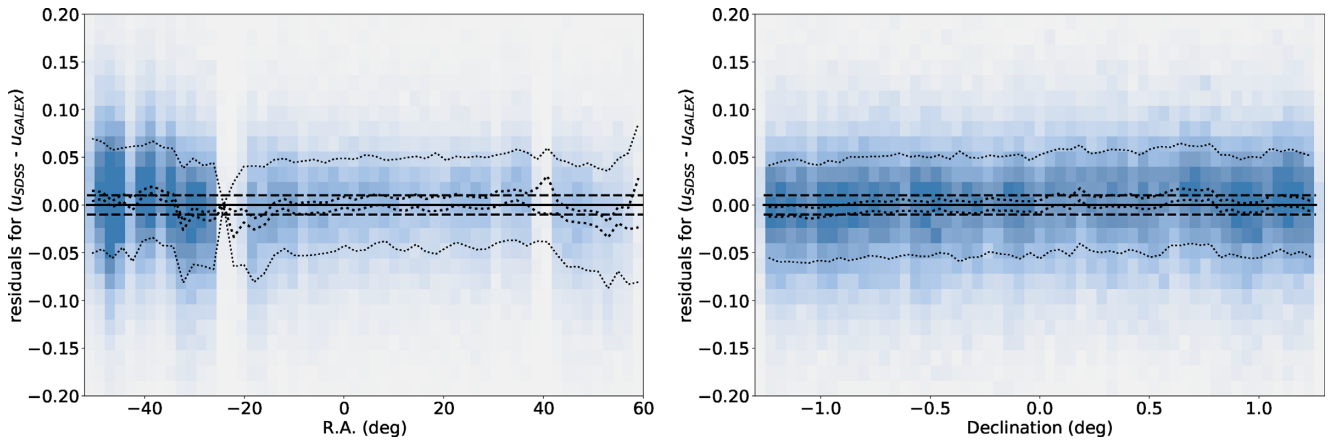
Figure 19. (Left-hand panel) Analogous to Fig. 6 (left-hand panel), except that here residuals between the SDSS *u*-band magnitudes and predicted *u*-band magnitudes transformed from the *GALEX* catalogue are shown. Unlike in Fig. 18, we exclude matches for which SDSS *u* > 20.0 The individual star scatter is 52.9 millimag (dot–dashed lines); the binned median scatter is 9.5 millimag (solid grey lines). (Right-hand panel) Analogous to Fig. 6 (right-hand panel), except that here the residuals between the SDSS *u*-band magnitudes and predicted *u*-band magnitudes transformed from the *GALEX* catalogue are shown. Unlike in Fig. 18, we exclude matches for which SDSS *u* > 20.0. The individual star scatter is 52.9 millimag (dot-dashed lines); the binned median scatter is 5.0 millimag (solid grey lines).

Table 5. Synthetic SDSS magnitudes for three WD dwarfs with *HST* photometry[a].

Name	RA	Dec.	u	g	r	i	z
GD50	57.2091083	− 0.975636	13.409	13.784	14.295	14.655	No data[b]
SDSSJ 232941.32+001107.8	352.4221875	0.185500	18.154	18.145	18.466	18.754	19.042
SDSSJ 010322.19-002047.7	15.8424625	− 0.346592	18.627	19.057	19.558	19.923	20.258

Notes. [a]Sourced from Bohlin et al. (2014) and Narayan et al. (2019).
[b]The CalSpec spectrum stopped at about 9000 Å and thus did not cover all of SDSS *z* band.

Table 6. AB offsets implied by three WD dwarfs with *HST* synthetic photometry[a].

	Δu	Δg	Δr	Δi	Δz
Mean	–	–	0.015	0.016	0.035
σ_{mean}	0.019	0.014	0.004	0.004	0.011

Note.[a] Offsets are defined as additive corrections to SDSS photometry to place it on AB scale (in mag). Listed values are unweighted mean and its uncertainty.

(2010). Our results for the synthetic SDSS AB magnitues for these three stars can be found in Table 5. The errors on these synthetic AB magnitudes are expected to be ∼5–10 millimag (statistical) and ∼10 millimag (systematic) (e.g. Bohlin et al. 2014).

Table 6 presents the numerical summary of the comparison between SDSS magnitudes and *HST*-based synthetic magnitudes for the three white dwarfs. We used unweighted mean because formal uncertainties for SDSS photometry are subdominant to systematic errors in the *HST*-based synthetic magnitudes, estimated to be ∼0.01 mag. Uncertainties of the mean offsets were computed from the observed scatter of the three values. In the *riz* bands, we detect significant (>3σ) deviations, ranging from 0.012 to 0.033 mag, while in the *u* and *g* bands, we can only place upper limits (at 2σ: 0.038 and 0.028 mag, respectively).

4 DISCUSSION AND CONCLUSIONS

To enable further progress in cosmological and other high-precision photometric measurements, modern multiband photometric sky surveys aim to deliver measurements internally consistent to at least the 1 per cent (0.01 mag) level. Over the last decade, a number of such large-scale surveys approached, and often surpassed this photometric accuracy requirement. For ground-based surveys, which are affected by variable atmospheric effects and hardware responses to changes in local environment (e.g. temperature), significant improvements are achieved by averaging multiple observations.

In this paper, we have described the construction, calibration, and testing of an updated version of the SDSS Stripe 82 Standard Star catalogue, I007 (Ivezić et al. 2007) that lists averaged SDSS photometry for about a million non-variable stars. Additional post-2007 SDSS data include about 2–3 times more measurements per star than in the original catalogue, resulting in 1.4–1.7 times smaller random photometric errors (precision) than in the original catalogue, and about three times smaller than individual SDSS runs.

Thanks to the availability of photometric data from recent wide-field surveys (*Gaia*, DES, Pan-STARRS, and CFIS), we were able to derive robust zeropoint corrections and establish that this new catalogue is superior to the original catalogue. Using a combination of comparisons to other catalogues and astrophysical constraints, we find that the contribution of the zeropoint errors to photometric uncertainties is <5 millimag for the *gri* bands, and <10 millimag for the *u* and *z* bands.

Various catalogue cross-comparisons have revealed minor problems with all the analysed catalogues. For example, we detected DES *z*-band zeropoint errors of up to 0.01–0.02 mag, as a function of RA, and demonstrated that the Gaia EDR3 *G* magnitude, G_{Gaia} has an overall gradient of ∼0.01 mag from the bright to faint end (16 ≤ G_{Gaia} ≤ 19), and therefore appears too faint by about 0.02 mag at G_{Gaia} ∼ 20.

We constrained offsets from the absolute AB magnitude scale using three white dwarfs with the *HST* CalSpec absolute photometry data. In the *riz* bands, we measured significant ($>3\sigma$) deviations, ranging from 0.015 to 0.035 mag (see Table 6), while in the *u* and *g* bands, we only placed upper limits (at 2σ: 0.038 and 0.028 mag, respectively). These constraints on absolute AB magnitude scale could be improved by increasing the number of such calibrators.

Thanks to its high stellar density, about 1 star arcmin^{-2}, and demonstrated sub-percent internal photometric precision, this catalogue is a good resource for both calibrating and testing other surveys. In particular, it will enable high-precision photometric testing of data collected during the commissioning phase of the Vera C. Rubin Observatory Legacy Survey of Space and Time.

All the catalogues generated as part of our work are made public and working links to freely access them have been provided in the Data Availability section. Please email the corresponding author for any queries or additional information.

SOFTWARE CITATIONS

(i) NUMPY (Harris et al. 2020)
(ii) MATPLOTLIB (Hunter 2007)
(iii) SCIPY (Virtanen et al. 2020)
(iv) ASTROPY (Astropy Collaboration et al. 2013, 2018)
(v) PANDAS (McKinney 2010)
(vi) ASTROML (VanderPlas et al. 2012).

DATA AVAILABILITY

The public data described here may be obtained from the following websites.

SDSS-IV, DR15:
http://www.sdss.org
https://dr15.sdss.org/sas/dr15/eboss/photoObj/
Gaia EDR3:
https://www.cosmos.esa.int/web/gaia/earlydr3
DES DR1:
http://datalab.noao.edu
MAST:
https://dx.doi.org/10.17909/T9RP4V

The catalogues generated as part of this work may be accessed at the following links:

New SDSS standard star catalogue, version 4.2:
http://faculty.washington.edu/ivezic/sdss/catalogs/stripe82.html
Old SDSS standard star catalogue, I007(version 2.6):
http://faculty.washington.edu/ivezic/sdss/catalogs/stripe82.html

REFERENCES

Abbott T. M. C. et al., 2018, ApJS, 239, 18
Agüeros M. A. et al., 2005, AJ, 130, 1022
Arenou F. et al., 2018, A&A, 616, A17
Astropy Collaboration et al., 2013, A&A, 558, A33
Astropy Collaboration et al., 2018, AJ, 156, 123
Betoule M. et al., 2013, A&A, 552, A124
Bianchi L., Conti A., Shiao B., 2014, Adv. Space Res., 53, 900
Bianchi L., Shiao B., Thilker D., 2017, ApJS, 230, 24
Blanton M. R. et al., 2017, AJ, 154, 28
Bohlin R. C., Gordon K. D., Tremblay P. E., 2014, PASP, 126, 711
Chambers K. C. et al., 2016, preprint (arXiv:1612.05560)
Dark Energy Survey Collaboration et al., 2016, MNRAS, 460, 1270
Doi M. et al., 2010, AJ, 139, 1628
Evans D. W. et al., 2018, A&A, 616, A4
Fabricius C. et al., 2016, A&A, 595, A3
Flaugher B. et al., 2015, AJ, 150, 150
Flewelling H. A. et al., 2020, ApJS, 251, 7
Frieman J. A. et al., 2008, AJ, 135, 338
Fukugita M., Ichikawa T., Gunn J. E., Doi M., Shimasaku K., Schneider D. P., 1996, AJ, 111, 1748
Gaia Collaboration et al.2021, A&A, 649, A1
Gaia Collaboration et al., 2016, A&A, 595, A1
Gaia Collaboration et al., 2018, A&A, 616, A1
Gunn J. E. et al., 1998, AJ, 116, 3040
Harris C. R. et al., 2020, Nature, 585, 357
Heinis S., Budavári T., Szalay A. S., 2009, ApJ, 705, 739
Honscheid K., DePoy D. L., 2008, preprint (arXiv:0810.3600)
Hunter J. D., 2007, Comput. Sci. Eng., 9, 90
Ibata R. A. et al., 2017, ApJ, 848, 128
Ivezić Ž. et al., 2004, Astron. Nachr., 325, 583
Ivezić Ž. et al., 2007, AJ, 134, 973 (I007)
Ivezić Ž. et al., 2019, ApJ, 873, 111
Kaiser N. et al., 2010, Proc. SPIE Conf. Ser. Vol. 7733, Ground-Based and Airborne Telescopes III. SPIE, Bellingham, p.77330E
Lindegren L. et al., 2018, A&A, 616, A2
Magnier E. A. et al., 2020a, ApJS, 251, 3
Magnier E. A. et al., 2020b, ApJS, 251, 5
Magnier E. A. et al., 2020c, ApJS, 251, 6
McKinney W., 2010, in van der Walt S., Millman J., eds, Proc. 9th Python Sci. Conf. Vol., 1, Data Structures for Statistical Computing in Python. Proceedings of the 9th Python in Science Conference 1 Austin, Texas, USA. 56
Morganson E. et al., 2018, PASP, 130, 074501
Morrissey P. et al., 2007, ApJS, 173, 682
Narayan G. et al., 2019, ApJS, 241, 20
Pier J. R., Munn J. A., Hindsley R. B., Hennessy G. S., Kent S. M., Lupton R. H., Ivezić Ž., 2003, AJ, 125, 1559
Riello M. et al., 2018, A&A, 616, A3
Schlegel D. J., Finkbeiner D. P., Davis M., 1998, ApJ, 500, 525
Smith J. A. et al., 2002, AJ, 123, 2121
Tucker D. L. et al., 2006, Astron. Nachr., 327, 821
VanderPlas J., Connolly A. J., Ivezić Ž., Gray A., 2012,Introduction to astroML: Machine learning for Astrophysics. Online Proceedings of Conference on Intelligent Data Understanding (CIDU} 1, p. 47,
Virtanen P. et al., 2020, Nature Meth., 17, 261
Waters C. Z. et al., 2020, ApJS, 251, 4
York D. G. et al., 2000, AJ, 120, 1579

This paper has been typeset from a TeX/LaTeX file prepared by the author.